Received: 15 September 2024 | Revised: 30 October 2024 | Accepted: 25 November 2024

DOI: 10.1002/dro2.162

RESEARCH ARTICLE

Droplet WILEY

Water-proofing mechanism of coupling structures observed in ladybird elytra and its bionic application

Jie Zhang[1,2] | **Hao Yang**[2] | **Jiannan Cai**[1] | **Junhao Shi**[2] | **Yuquan Zheng**[2] | **Hamed Rajabi**[3] | **Jieliang Zhao**[4] | **Jianing Wu**[1,2]

[1]School of Advanced Manufacturing, Sun Yat-Sen University, Shenzhen, China

[2]School of Aeronautics and Astronautics, Sun Yat-Sen University, Shenzhen, China

[3]Division of Mechanical Engineering and Design, School of Engineering, London South Bank University, London, UK

[4]School of Mechanical Engineering, Beijing Institute of Technology, Beijing, China

Correspondence
Hamed Rajabi, Division of Mechanical Engineering and Design, School of Engineering, London South Bank University, London, SE1 0AA, UK.
Email: rajabijh@lsbu.ac.uk

Jieliang Zhao, School of Mechanical Engineering, Beijing Institute of Technology, Beijing 100081, China.
Email: jielzhao@bit.edu.cn

Jianing Wu, School of Advanced Manufacturing, Sun Yat-Sen University, Shenzhen 518107, China.
Email: wujn27@mail.sysu.edu.cn

Funding information
Shenzhen Science and Technology Program, Grant/Award Numbers: GXWD2021B03, 20220817165030002; National Natural Science Foundation of China, Grant/Award Numbers: T2422031, 52275298; Postdoctoral Fellowship Program of CPSF, Grant/Award Number: GZC20240192

Abstract

Ladybirds (*Coccinella septempunctata*) are adept at living in humid conditions as their elytra can effectively shield their bodies from raindrops. However, due to technical difficulties in examining the delicate structure, the understanding of the water-proofing mechanism of the coupling structure and its impact on the dome-like elytra response to the raindrops remain elusive. In this combined experimental and theoretical study, we showed that the coupling structure on the ladybird elytra can ward off the raindrops traveling at a velocity of 6 m/s, which generates an impact force equivalent to 600 times the body weight. The waterproofing mechanism relies on the deformability of the elytra and their microstructures, which collectively impedes the formation of microchannels for liquids. The enhanced water-proofing capabilities enabled by the coupling structures are validated through experimental testing on comparative 3D-printed models, showing the effectiveness of these structures in improving water resistance. Subsequently, we showcased a water-proofing device, which substantially improved the efficiency of solar panels in converting solar energy. This multidisciplinary study not only advances our understanding of the biomechanics of coupling systems in insects but also inspires the design of water-proofing deployable structures.

INTRODUCTION

Water, as a vital conveyor of nutrients and oxygen to every cell within organisms, is essential for life.[1] For some insects, however, possessing the ability to repel water is crucial as it not only dictates the ecological niches they inhabit but also greatly enhances their adaptability to different environmental conditions. The water-proofing ability is significant to their survival and success across diverse habitats.[2–5] This demand has prompted insects to evolve diverse hydrophobic structures to induce water resistance, such as the wings of butterflies (*Parnassius glacialis*) coated in dense scales and the legs of water striders (*Aquarius remigis*) with needle-shaped microstructures.[6–8]

Jie Zhang and Hao Yang contributed equally to this study.

As one of the most diverse insect orders, beetles also possess various water-proofing strategies to meet different functional requirements. Leaf beetles (*Gastrophysa viridula*) are able to walk freely underwater by using air bubbles trapped between adhesive hairs in the legs; hairs can wet the substrate and produce capillary adhesion.[9] Diving beetles (*Dytiscidae*), as typical aquatic insects, can breathe underwater, benefiting from an air bubble attached to the surface through respiratory pores in their integument for warding off the water.[10] Although beetles have diverse strategies to deal with the humid environments in which they live, they share some common features, one of which is possessing multifunctional hard dome-like elytra, which are the first line of defense against environmental hazards.[11] The internal sandwiched structure of the elytra, for example, shows outstanding mechanical properties to resist drastic impacts.[12] The elytra can be locked together by a coupling structure consisting of a mortise and a tenon, where the blade-shaped tenon is inserted into the grooved mortise structure.[13] These structures provide their fragile hindwings and flexible body with a protective cover to prevent contamination.[14–16] In addition, the scoop-shaped elytra attach to the body by a membrane between the tergum and pleuron, and when disturbed by predators, the beetles can deploy their elytra and flap hindwings to escape swiftly.[17,18]

In addition to the above functions, beetle elytra are covered by waxes that enable them to become hydrophobic.[19] The reason why the cuticle exhibits a capability of low permeability to water is an organized monolayer of grease.[20] However, despite the discontinuous structure and natural suture exhibited by the elytra system resulting from its deployment properties, the coupling mechanism of the elytra is not inherently susceptible to water penetration and may effectively repel water, providing protection. Intriguingly, although the disabled water-proofing system may pose a huge challenge to beetles, there have been scarcely related reports yet on the water-proofing failure of beetles even the presence of coupling structures. This may imply that the elytra, and specifically the structures by which they are connected to each other have undergone adaptations that prevent water penetration.

Here, we took a ladybird (*Coccinella septempunctata*) as an example to investigate the water-proofing mechanism of coupling structures by combining both experimental and theoretical studies. The wide distribution and complex habitat globally make the ladybirds be likely to encounter rainy conditions regularly.[21–23] Previous studies on flying insects have validated that rain increases their energetic cost of movement, and dampened hindwings may be detrimental to the flight of ladybirds.[24] In a potentially much worse case, the impact of a raindrop with a mass close to a ladybird (~30 mg) will promote rainwater infiltration.[25] Therefore, a fine sealing performance of elytra may be of great essentiality for a ladybird survival. While the wettability of the elytra has been extensively studied, the response and sealing performance of the elytra after impact with raindrops has received little attention.[26,27] To understand the role of the coupling structures in water-proofing, we combined both high-speed filming and dynamic analysis to uncover the physics of a free-falling waterdrop impacting the elytra of a ladybird. We discovered that the coupled elytra function as a watertight shell to prevent infiltration of liquid even with the occurrence of impact as much as 600 times body mass of the insect. By employing computational fluid dynamics (CFD) analysis, we simulated the collision of a waterdrop with the coupling structure to assess the critical contact stresses on the contact surfaces, and investigated the influence of the geometry of the coupling structure on sealing performance. This work may not only sketch a more complete frame to illustrate function of elytra coupling of a beetle, but inspire the water-proofing devices with long connecting lines applied in rainy environment.

RESULTS AND DISCUSSION

We filmed the collision between the varying-volumed droplets ranging from 5 to 45 μL and the ladybird elytra with a high-speed camera, as illustrated in Figure 1a. Then, the impact force generated by these droplets is measured while falling from a height of 600 mm onto ladybirds, as shown in the dashed box of Figure 1a. High-speed snapshots demonstrate that the droplet is shaped circular when in contact with the elytra and then begins to deform and spread (Figure 1b). At 1.56 ms, the movement of the droplet edge reverses, retracting toward the top of the elytra. As shown in Figure 1b, the average contact angle of the droplet on the elytra reaches 109.23 ± 5.31°, which indicates that the elytra surface exhibits hydrophobic characteristics for repelling water. Then, we measured the mass of these droplets m_d = 5–45 mg and evaluated the impact velocity as V_d = 4.10 ± 0.90 m/s, based on which the impact force associated with the transfer of momentum could be calculated as ~180 mN, analogous to 600 times the weight of the ladybird samples. We considered that such a drastic collision force would cause the droplets to break through the elytra and impact their fragile hind wings and flexible abdomens (Supporting Information: Video S1). However, the living ladybirds with naturally closed elytra can maintain a tight seal, effectively preventing droplets from contacting their bodies. Hence, we considered that the coupling structure that connects the elytra pair may play a water-proofing function for enhancing their survival in rainy environments. To validate this, we repeated the above experiments after using micro-polishing tools to remove the coupling structure of the of ladybird elytra (Figure 1c). In the comparative experiments, we noticed the presence of dyed liquid on the inner surfaces of the elytra and the upper surfaces of the folded hind wings, which suggests that the elytra without coupling structure are unable to withstand the impact of the droplets, leading to penetration by the droplets. Here, we first demonstrated that the existence of the coupling structures can effectively hold up droplets outside the elytra, thus ensuring dryness of the hind wings.

To illustrate the effect of the coupling structures on warding off droplets, we built a mathematical model to simulate the physical interactions in the absence of coupling structure. We measured the gap width H_g between the tenon and mortise structures, discovering that the width usually ranges from 6 to 10 μm (Figure 1d). Here, D is the vertical distance from a measured point to the coordinate origin o. Since the surface tension of the water–air interface γ = 0.07 N/m, we further derived the Laplace pressure as P_L = 3.83 kPa (Figure 1e). To avoid the droplets entering the elytra, the dynamic pressure P_D

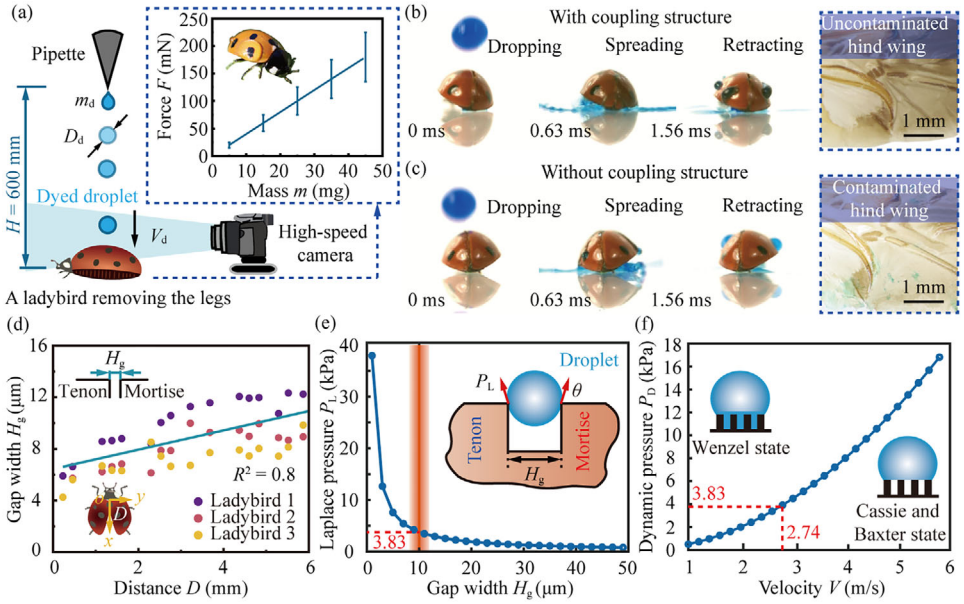

FIGURE 1 Collision between water drops and the elytra. (a) Schematic of dyed droplet impact experiment. The dyed droplet impacts the natural elytra (b) and the elytra without coupling structure (c). (d) Gap width H_g between the tenon and mortise structures. (e) Laplace pressure P_L generated by the droplets. (f) Dynamic pressure P_D caused by impact velocity V.

should satisfy $P_D < P_L$, that is, the impact velocity V_d being smaller than 2.74 m/s (Figure 1f). However, the impact velocity of the raindrop in nature is 6–9 m/s, much greater than this critical velocity. Hence, the elytra without the coupling structure cannot keep the droplets out of the body, which indicates that the coupling structures of the elytra system play an essential role in the water-proofing of the elytra.

To uncover the water-proofing mechanism, we focused on the collision of a droplet on the coupling structures by CFD. According to anatomy of the ladybird elytra, we designed a simplified model of the elytra, and divided the contact region between the mortise and tenon into upper R_u, middle R_m, and lower R_l regions.[13] As demonstrated in Figure 2a, we simulated the collision of a droplet with elytra to understand how the coupling structure of elytra can affect the sealing performance in the collision. After it contacts the topical center of the elytra at a velocity of 4 m/s, the droplet rapidly spreads to cover the full elytra within 1.50 ms. The droplet flows down the surface of the elytra as the effect of inertia force, consistent with the experimental phenomenon of the droplets colliding with the elytra of a ladybird. This numerical result can be applied to further analyze the impact of the coupling structure on water-proofing capacity. As shown in the lower panel of Figure 2a, we discovered that the droplet infiltrates into the regions of both R_u and R_m, while no change in liquid volume fraction is found in the region R_l, which may cause the difference in the pressure of the liquid in these three regions of the gap.

When the droplet infiltrates a radius of R_u, the volume fraction of liquid reaches a maximum value of 0.90 at 1 ms and then declines to 0 rapidly. In the region R_m, the volume fraction of liquid begins to increase at 0.5 ms, reaching a maximum value of 0.36 at 2 ms, occupying only 0.40 that of the region R_u (Figure 2b). Compared to the above regions, the volume fraction of liquid in region R_l remains approximately constant at 0, which indicates that the droplet cannot enter this region. In response to the infiltration into the gap regions, the intrusion of water elevates the fluid pressure in regions R_u and R_m by 13.4 and 11.6 kPa at 0.5 ms, respectively. In contrast, the fluid pressure in R_l consistently remains negligible, hovering around 0 kPa (Figure 2c). Both the volume fraction and pressure of the liquid in the gap suggest that, although the droplet infiltrates into the upper and middle regions after colliding the coupling structure of the elytra, it fails to enter the region R_l.

To further elucidate the physical mechanism of this water-proofing phenomenon, we built a global coordinate system *o-xyz*, and quantified the local small displacement of points T_i and M_j (i, j = 1, 2, 3) on the tenon and mortise structures, respectively. Figure 2d first demonstrates that both horizontal and vertical displacements of the points T_i (i = 1, 2, 3) on the tenon reach their maximum value in 0.5 ms, following which they rapidly return to their original positions. The vertical displacement of the tenon at each region of the gap is greater than the horizontal displacement, with a maximum of –0.44 μm in region R_m and a smaller value of –0.33 μm in R_u and R_l. The horizontal displacement of the tenon in region R_u is 0.03 μm along the *X*-axis, while that of the tenon in R_m and R_l are opposite, as –0.05 and –0.13 μm, respectively, indicating that the upper region of the gap tends to become narrow upon impact, while the middle and lower regions tend to become more expansive. However, the vertical displacement of the mortise is less than that of the tenon, with a maximum value of only 0.21 μm, where the displacement in regions R_u and R_l is greater than that in region R_m. Then, we further evaluated the horizontal displacement of the points on the mortise structure, as –0.02, 0.04, and 0.08 μm, respectively, which exhibits a similar trend as the tenon, both narrowing the upper region and widening the middle and lower regions. Here, we also discovered that the tenon experiences greater deformation compared to

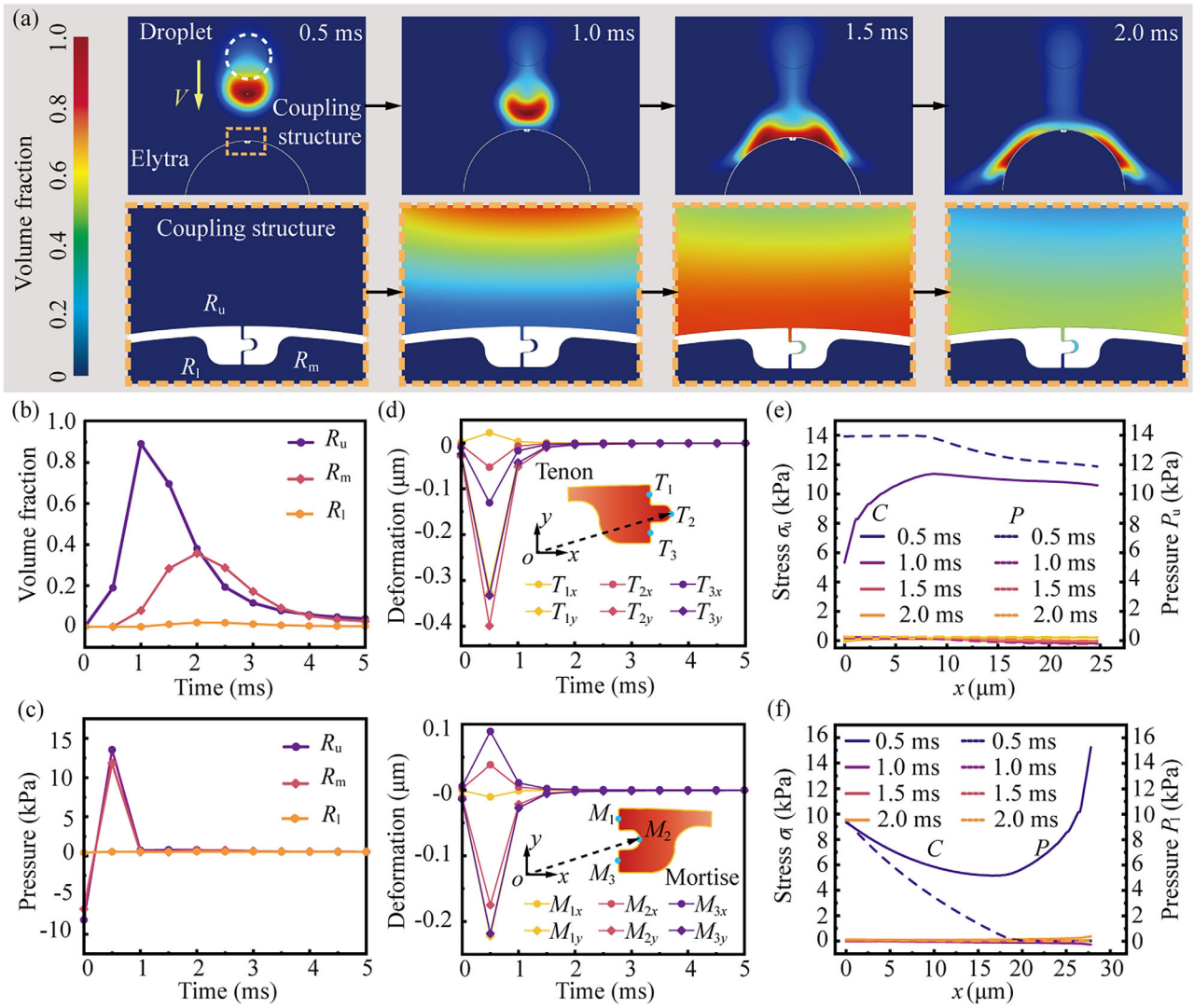

FIGURE 2 Simulation of a droplet impacting on ladybird elytra. (a) Snapshots of numerical simulation. (b) Volume fraction of the regions. (c) Liquid pressure of the regions. (d) Deformation of the points, including T_i and M_j ($i, j = 1, 2, 3$) on both tenon and mortise structures. Comparison of the contact stress σ and liquid pressure P on the upper (e) and lower (f) contact surfaces of the tenon structure.

the mortise. This different vertical motion of the tenon and mortise structures enables the lower contact surface of the tenon to adhere more closely to the mortise than the upper contact surface, which may increase the contact stress on this surface to improve sealing performance. This may explain the difference in fluid volume fraction and fluid pressure within the three regions of the gap.

To verify this hypothesis, we further calculated both the contact stress σ and the fluid pressure P on the contact surface. During collision, the stress σ on the upper (Figure 2e) and lower (Figure 2f) surfaces maximizes at the point of maximum deformation. Specifically, the stress σ_u on the first half of the upper surface rises from 5.30 to 11.40 kPa, and then stabilizes around 10.90 kPa in the second half, as shown in Figure 2e. By contrast, the fluid pressure P_u achieved by the droplet is always greater than the stress σ_u caused by contact, so that the water easily enters the region R_u. In terms of the lower contact surface, the stress σ_l and fluid pressure P_l exhibit opposite trends toward Figure 2e, which is depicted in Figure 2f. For example, the stress σ_l on the lower surface first declines from 9.30 to 5.20 kPa and then rises from the midpoint of the surface to 15.20 kPa, consistently greater than the fluid pressure P_l decreasing from 9.5 to 0 kPa. Hence, the lower contact surface of the coupling structure offers superior sealing performance compared to the upper contact surface directly upon the impact of a droplet.

We applied micro-computed tomography (micro-CT) to scan a ladybird, by which the elytra system can be obtained, as shown in Figure 3a. Here, the tenon of the coupling structure presents an upwarp profile with an angle of $\alpha_0 = 3.40 \pm 0.30°$, and the radius of its tip can be measured as $r_0 = 22.50 \pm 1.70$ μm. Then, we also explored effects of the geometry of the coupling structures on the sealing performance by varying r_0 and α_0, and defined the variation of radius r/r_0 and angle α/α_0 to reflect trends in geometric parameters (Figure 3b). Figure 3c illustrates the contact stress distribution on the lower contact surface

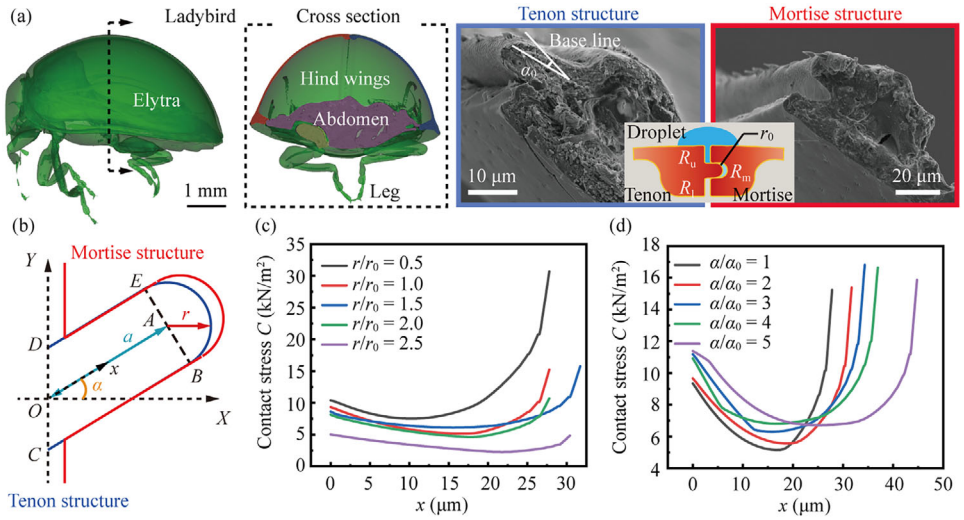

FIGURE 3 Effects of geometrical parameters of coupling structures on sealing performance. (a) Micro-computed tomography (micro-CT) and microstructure images of ladybird. (b) Geometrical parameters of the coupling structure with the radius r and angle α. Contact stress on the upper contact surface of the coupling structure related to radius (c) and angle (d) of the tenon structure.

as r/r_0 increases from 0.5 to 2.5. Here, we neglected the larger range of r because the thickness of the raised part of the tenon is already greater than the coupling structure when r/r_0 gets more than 2.5. The contact stress distribution is comparable for lower contact surfaces with different r, with a tendency to increase along the X-axis, reaching a maximum at the end. The contact stress C on the lower contact surface reduces with increasing r, and the maximum contact stress at $r/r_0 = 0.5$ is 30.3 kN/m^2, six times that at $r/r_0 = 2.5$. In addition, the tenon slopes further upward as α increases; therefore, the contact area of the lower contact surface is widened (Figure 3d). By contrast, contact stress C tends to increase with an ascending angle α, while the maximum contact stress varies little, which reaches a maximum of 16.8 kN/m^2 at $\alpha/\alpha_0 = 3$, which is only 10% greater than that at $\alpha/\alpha_0 = 1$. Based on the simulation results, we fit the trend of the maximum contact stress on the lower surface under the combined influence of r and α. The maximum contact stress is greater on the lower surface of the less angular coupling structure, and reduced on thicker and more angled ones. However, when r and α are small, the stresses on the contact surface are greater with a maximum of 58.2 kN/m^2, indicating that in this shape the coupling structure may be susceptible to fracture upon impact. Hence, to meet the dual functional requirements of both sealing performance and structural stability of the coupling structure, ladybirds may possess a more conservative geometry, aligning with the microstructures measured through micro-CT images.

According to the actual geometry of the elytra, we developed two comparative models to further show the role of coupling structures played in water-proofing. As depicted in Figure 4a, the tenon and mortise structures are marked in blue and red, respectively. For the convenience of fabrication, we enlarged the structures in Solidworks five times, and utilized our equipment (microArch S130, BMF Precision Tech Inc.) to 3D-print these models using photosensitive resin (SOMOS Imagine 80000/SOMOS GP Plus). The gap between the two elytra can be observed under a microscope (Olympus, CX33), as shown in Figure 4a (i and ii). To better demonstrate the influence of the coupling structure on the water-proofing performance of the elytra, we attached a pH indicator paper to the internal surface of the models. Here, we first ensured that the spacing between mortise and tenon structures in the comparative models is consistent. Due to the absence of coupling structures, we observed that there are small gaps between the mortise and tenon structures in the first model. Subsequently, we applied a pipette to drop the $NaHCO_3$ solution (~5 mL) at a height of 30 cm from the ground toward the coupling structures. The dome-like elytra facilitate the downward movement of droplets upon contact, positively influencing their dispersion (Supporting Information: Video S2). We found that only a minimal amount of liquid exists on the external surface of the models (Figure 4b). In addition, in terms of the model with coupling structure, the color of the indicator paper still remains yellow. By contrast, the droplet impact on the model without coupling structures led to a little of the liquid penetrating its interior, causing the indicator paper to change color from yellow to purple. These findings show that the presence of coupling structure effectively prevent high-velocity droplets from contaminating the elytra.

This water-proofing mechanism is of great significance for developing deployable devices that ensure the efficient operation of solar panels. These facilities enable renewable energy generation, reducing reliance on fossil fuels and contributing to a more sustainable energy system; however, exposed panels for a long time are often covered with a layer of dust. When it rains, the rainwater will fuse with the dust on the solar panels, resulting in large-scale stains that affect energy conversion efficiency. Derived from coupling structures, we proposed a water-proofing deployable device with binary states, that is, open and closed states, to prevent the dust from mixing with rainwater, as shown in Figure 4c. This device is composed of two motors (MG90, RXHC), a solar panel, a support structure, and an elytra system. Here, the elytra system can be actuated by the motors, which are modulated by a microcontroller (UNO, Arduino). Since the closed elytra system can

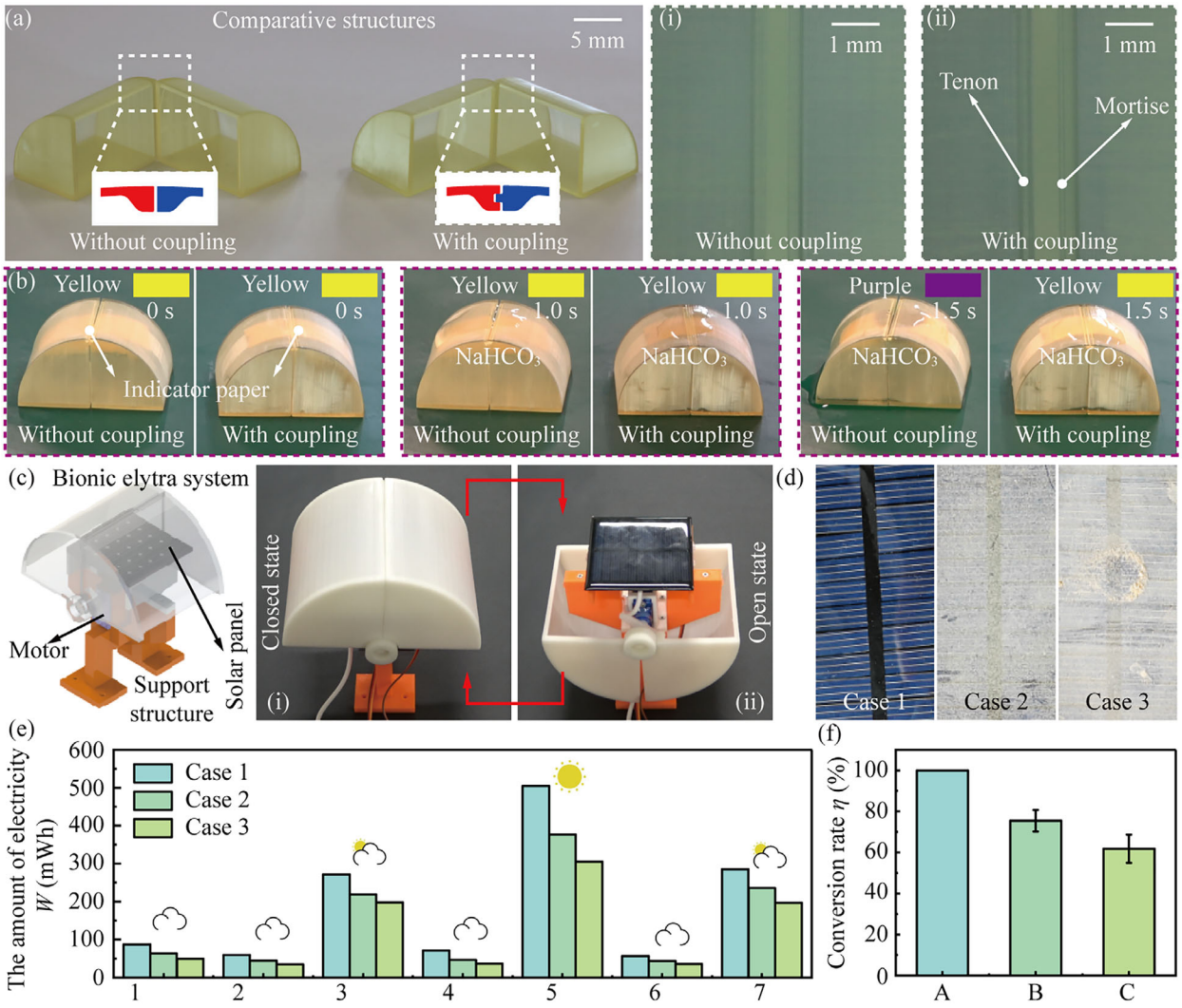

FIGURE 4 Three-dimensional-printed biomimetic structures in potential application. (a) Morphology of comparative models. (b) Comparison of color reactions of indicator papers. (c) A water-proofing deployable device. (d) Three solar panels in clean, dusty, and stained conditions. (e) Electricity generated of the cases in 1 week. (f) Energy conversion rate of solar panels of the three cases.

prevent rainwater from mixing with the dust, the energy conversion efficiency will be improved. To validate this, we continuously measured the amount of electricity generated by the solar panels in clean, dusty, and stained conditions in a week, denoted as cases 1–3 (Figure 4d,e). Here, we assumed that, for the clean solar panels, we had conversion rate $\eta = 100\%$, and η of the rest of the two cases compared to case 1 can be further evaluated. We discovered that η reaches $75.45 \pm 5.26\%$ of case 1 when the solar panel is covered with dust (Figure 4f). If the solar panels are contaminated by the stain formed by contact between dust and rainwater (i.e., case 3), η will reduce to $61.75 \pm 6.84\%$. Our bio-inspired device can therefore effectively prevent the solar panel from being further stained, by which η can be improved compared to case 3.

CONCLUSION

In this study, we combined both experimental and theoretical methods to elaborate the water-proofing mechanism of coupling structures bearing on ladybird elytra. The coupling structures can enable the elytra to become seamless covers, thereby providing their hindwings with effective protection to prevent contamination from raindrops permeating into them. In addition to ladybirds, such a mechanism achieved by coupling structures may also exist in other beetle species. Then, inspired by such a mechanism, we developed a waterproof and deployable device for solar panels. The experimental results show that our device can improve the energy conversion rate of solar panels. Although significant advancements have been made to improve the energy conversion efficiency of solar panels by preventing the blend of dust and water, the approach alone are insufficient to meet the performance requirements of modern energy systems fully. In future study, we would like to address this challenge by integrating a self-cleaning mechanism within the bionic elytra system, by which the dust can be removed from the solar panels during the opening process.[28] By incorporating such a self-cleaning feature, we anticipate a remarkable enhancement in the efficiency of energy conversion, thereby optimizing its performance and extending its operational lifespan.

METHODS

We bred ladybird samples (*C. septempunctata*) indoors in an insect cage in Shenzhen, Guangdong Province, China, and all ladybirds were fed with aphids (*Megoura japonica*) living on broad bean seedlings (*Vicia faba L.*). We measured the body mass m_L of the ladybird samples ($n = 20$) on a scale (Quintix35-1CN, Sartorius). The width w and height h of each ladybird sample were evaluated by using a Vernier caliper (AIRAJ 1331, AIRAJ). Here, these geometrical parameters were defined as the maximum distance along the short and long axes of the body in the plane perpendicular to the abdominal plane, respectively.

We built an experimental setup composed of an acrylic sheet with hydrophobic surface treatment, a micro-pipette, and a high-speed camera to observe the collision of droplets and the elytra. The camera (Phantom, Micro CLY310) equipped with a macro lens (Canon, EF100mmf/2.8LISUSM) was employed to record the kinematics of the droplets at 3200 fps. Prior to each experiment in the laboratory, the ladybirds were first anesthetized by freezing and placed horizontally with the abdomen facing downward on the experimental setup. To film the movement, the droplets were colored blue by the stain. Then, a series of dyed droplets at 5–45 μL with 10-unit intervals (volume increment: 10 μL) fell freely toward the center of the ladybirds from a height of 600 mm. To ensure whether the droplets infiltrated into the interior of the elytra and contaminated the hind wings and/or abdomens, we dissected the elytra and hind wings of the ladybirds impacted by droplets. By a device composed of a camera (Canon, EOS 6D) and a microscope (Olympus, CX33), the internal surface of the elytra and the hindwings being infiltrated with liquid were visualized. For comparison, the elytra of these ladybirds were also opened after anesthesia to remove the coupling structure, and then the experimental procedure was repeated.

Two wetting states could be observed on surfaces with microstructures, that is, Cassie (wetting) and Wenzel (nonwetting).[29] A wetting liquid would fill the microstructures, while a nonwetting liquid may not penetrate surface cavities, forming air pockets and leading to a composite solid–air–liquid interface.[30] Here, we built a mathematical model to determine the wetting state of the gap between elytra and droplets. When droplets with a radius of R_d impacted on the width of the gap H_g between the elytra, the state of wetting depended on the balance of wetting pressure (i.e., dynamic pressure P_D) and antiwetting pressure (i.e., Laplace pressure P_C). Specifically, neglecting the viscous effect, the dynamic pressure $P_D = 1/2\rho V^2$ acting on the liquid interface could be calculated when droplets hit microstructures, pushing the liquid interface downward.[31] Here, ρ and V are expressed as density and velocity, respectively. Hence, the elytra experienced impact force $F_D = P_D A_l$ by the liquid-free surface with an area of A_l enclosed by the gap and elytra. At mechanical equilibrium, this force was balanced by the capillary force $F_C = 2\sqrt{R_d^2 - (1/2H_g)^2}\gamma\cos\theta$ applied at the top of the gap, in which θ and γ were average contact angle defined on the contact surface and the surface tension of the liquid–air interface, respectively. When the two forces were in balance $F_D + F_C = 0$, the critical wetting pressure could be denoted as the Laplace pressure, that is, $P_C = 2\gamma\cos\theta/H_g$.[32] By comparing the above two pressures, we could determine whether the droplets have infiltrated the gap.

To observe the state of the coupling structure when the elytra were closed, we used an Xradia Micro XCT-400 (Xradio Inc.). Ladybird samples ($n = 4$) mounted on a sample holder were scanned at a voltage of 60 kV and a current of 133 μA with a resolution of 5 μm. For each ladybird, we gained about 1000 photos, and then processed these images using the PITRE and Mimics software (Materialise). Based on these images, we measured the gaps between the coupling structure, and quantified the geometry of the coupling structure precisely. To describe the dimension of the gap and the geometry of elytra, we set a local coordinate system with the scutellum as the origin O. The X-axis started from point O toward the posterior, and the Z-axis arrowed toward the abdomen. Then, the Y-axis was determined by the right-hand rule.

Scanning electron microscopy (SEM) is applied to observe the microstructure of coupling structures between the elytra of the ladybirds. The fresh samples ($n = 5$) are fixed by soaking in 2.50% glutaraldehyde for 3 h at 26°C. These samples are then cleaned with 0.10 mol/L phosphate buffer (pH 7) for 20 min, and dehydrated through an ascending ethanol series (at 75%, 80%, 85%, 90%, 95%, and 100% for 12 h) before freeze drying. We mounted the processed samples on SEM stubs with graphite adhesive tape. After being coating in gold palladium, the samples can be examined under a SEM (FEI Quanta 200) in high-vacuum mode at 15 kV.

Atomic force microscopy (AFM) was used to characterize the mechanical properties of the coupling structure. A piece of elytron with the coupling structure ($n = 5$) was removed by a scalpel under a microscope, and then placed perpendicularly on a glass slide. A probe (RTESPA-150, BRUKER) with a testing range of 50 MPa–50 GPa was used with a Dimension Icon AFM (FastScan, BRUKER) to measure the Young's modulus E of the elytra. Each elytra sample was mounted to the sample stage and tested at three sampling points along the length of each sample. In the peak force tapping mode, the vibrating tip performed vertical indentation to record force curves for each sampling point on the surface of the specimens. By real-time analysis of the force curves, the Young's modulus of each sampling point could be gained and averaged by fitting with Derjaguin, Muller, and Toporov model. This experimental result can be applied while conducting numerical simulations.[13]

ACKNOWLEDGMENTS

This work was supported by the Shenzhen Science and Technology Program (grant numbers GXWD2021B03 and 20220817165030002), the National Natural Science Foundation of China (grant numbers T2422031 and 52275298), and the Postdoctoral Fellowship Program of CPSF (grant number GZC20240192). We thank Dr. Li Gong from Instrumental Analysis & Research Center of Sun Yat-Sen University for assistance in measuring the Young's modulus of elytra. We thank Caixia Gao and Xiaowei Qin from Institute of Zoology, Chinese Academy of Sciences, for CT scanning and freeze-drying. We thank Lixin Gong from

School of Aeronautics and Astronautics, Sun Yat-Sen University, for assistance in conducting experiments.

CONFLICT OF INTEREST STATEMENT

The authors declare no conflicts of interest.

ORCID

Jianing Wu https://orcid.org/0000-0003-0902-4466

REFERENCES

1. Hossain MZ. Water: the most precious resource of our life. *Global J Adv Res*. 2015;2:1436-1445.
2. Suzuki C, Takaku Y, Suzuki H, et al. Hydrophobic-hydrophilic crown-like structure enables aquatic insects to reside effectively beneath the water surface. *Commun Biol*. 2021;4:708.
3. Suter RB, Stratton GE, Miller PR. Taxonomic variation among spiders in the ability to repel water: surface adhesion and hair density. *J Arachnol*. 2004;32:11-21.
4. Bush JWM, Hu DL, Prakash M. The integument of water-walking arthropods: form and function. *Adva Insect Physiol*. 2007;34:117-192.
5. Beament J. The waterproofing mechanism of arthropods: II. The permeability of the cuticle of some aquatic insects. *J Exp Biol*. 1961;38:277-290.
6. Byun D, Hong J, Ko JH, et al. Wetting characteristics of insect wing surfaces. *J Bionic Eng*. 2009;6:63-70.
7. Gao X, Jiang L. Water-repellent legs of water striders. *Nature*. 2004;432:36.
8. Perez Goodwyn P, Wang J, Wang Z, Ji A, Dai Z, Fujisaki K. Water striders: the biomechanics of water locomotion and functional morphology of the hydrophobic surface (Insecta: Hemiptera-Heteroptera). *J Bionic Eng*. 2008;5:121-126.
9. Hosoda N, Gorb SN. Underwater locomotion in a terrestrial beetle: combination of surface de-wetting and capillary forces. *Proc R Soc B Biol Sci*. 2012;279:4236-4242.
10. Madsen BL. Submersion respiration in small diving beetles (Dytiscidae). *Aquatic Insects*. 2012;34:57-76.
11. Sun M, Liang A, Watson GS, Watson JA, Zheng Y, Jiang L. Compound microstructures and wax layer of beetle elytral surfaces and their influence on wetting properties. *PLoS One*. 2012;7:e46710.
12. Sun M, Appel E, Kovalev A, Gorb E, Liang A, Gorb SN. The influence of the topography and physico-chemical properties of the cuticle surface on the wettability and adhesive properties of the elytra of the dung beetle *Geotrupes stercorarius* (Coleoptera, Scarabaeidae). *Bioinspir Biomim*. 2017;13:016008.
13. Zhang J, Yuan Q, Jiang Y, et al. Elytra coupling of the ladybird *Coccinella septempunctata* functions as an energy absorber in intentional falls. *Bioinspir Biomim*. 2021;16:056018.
14. Frantsevich L. Experimental evidence on actuation and performance of the elytron-to-body articulation in a diving beetle, *Cybister laterimarginalis* (Coleoptera, Dytiscidae). *J Insect Physiol*. 2012;58:1650-1662.
15. Song Z, Yan Y, Tong J, Sun J. Asian ladybird folding and unfolding of hind wing: biomechanical properties of resilin in affecting the tensile strength of the folding area. *J Mater Sci*. 2020;55:4524-4537.
16. Baek S, Yim S, Chae S, Lee D, Cho K. Ladybird beetle–inspired compliant origami. *Sci Robot*. 2020;5:eaaz6262.
17. Burgio G. Ecology and behaviour of the ladybird beetles (Coccinellidae). *Eur J Entomol*. 2013;110:94.
18. Zhang J, Li J, Li C, Wu Z, Liang H, Wu J. Self-righting physiology of the ladybird beetle *Coccinella septempunctata* on surfaces with variable roughness. *J Insect Physiol*. 2021;130:104202.
19. Wigglesworth V. The epicuticle in an insect, *Rhodnius prolixus* (Hemiptera). *Proc R Soc Lond Ser B-Biol Sci*. 1947;134:163-181.
20. Beament J. The waterproofing mechanism of arthropods: I. The effect of temperature on cuticle permeability in terrestrial insects and ticks. *J Exp Biol*. 1959;36:391-422.
21. Dai Z, Yang Z. Macro-/micro-structures of elytra, mechanical properties of the biomaterial and the coupling strength between elytra in beetles. *J Bionic Eng*. 2010;7:6-12.
22. Faizul H, Sardar AM, Kausar S, Shamsur R. Diversity and distribution of ladybird beetles in District Dir Lower, Pakistan. *Int J Biodivers Conserv*. 2011;3:670-675.
23. Akhavan E, Jafari R, Vafai R, Afrogheh S. Biodiversity and distribution of predaceous ladybird (Coleoptera: Coccinelliae). *Int Res J Appl Basic Sci*. 2013;5:705-709.
24. Dickerson A, Shankles P, Madhavan N, Hu D. Mosquitoes survive raindrop collisions by virtue of their low mass. *Proc Natl Acad Sci U S A*. 2012;109:9822-9827.
25. Yarin A. Drop impact dynamics: splashing, spreading, receding, bouncing. *Annu Rev Fluid Mech*. 2006;38:159-192.
26. Sun M, Liang A, Watson G, Watson J, Zheng Y, Jiang L. Microstructure and wettability on the elytral surface of aquatic beetle. *Appl Mech Mater*. 2014;461:731-740.
27. Godeau G, Godeau R, Orange F, Szczepanski C, Guittard F, Darmanin T. Variation of *Goliathus orientalis* (Moser, 1909) elytra nanostructurations and their impact on wettability. *Biomimetics*. 2018;3:6.
28. Zhang W, Jiang W, Zhang C, et al. Honeybee comb-inspired stiffness gradient-amplified catapult for solid particle repellency. *Nat Nanotechnol*. 2024;19:219-225.
29. Li H, Zhang K. Dynamic behavior of water droplets impacting on the superhydrophobic surface: both experimental study and molecular dynamics simulation study. *Appl Surf Sci*. 2019;498:143793.
30. Ren L, Kim C, Wang Z. Small droplet, big world. *Droplet*. 2022;1:1.
31. Deng T, Varanasi K, Hsu M, et al. Nonwetting of impinging droplets on textured surfaces. *Appl Phys Lett*. 2009;94:133109.
32. Bartolo D, Bouamrirene F, Verneuil E, Buguin A, Silberzan P, Moulinet S. Bouncing or sticky droplets: impalement transitions on superhydrophobic micropatterned surfaces. *Europhys Lett*. 2006;74:299.

SUPPORTING INFORMATION

Additional supporting information can be found online in the Supporting Information section at the end of this article.

How to cite this article: Zhang J, Yang H, Cai J, et al. Water-proofing mechanism of coupling structures observed in ladybird elytra and its bionic application. *Droplet*. 2025;e162. https://doi.org/10.1002/dro2.162